

# The last orbit of binary black holes

M. Campanelli, C. O. Lousto, and Y. Zlochower

*Department of Physics and Astronomy, and Center for Gravitational Wave Astronomy,  
The University of Texas at Brownsville, Brownsville, Texas 78520*

(Dated: November 8, 2018)

We have used our new technique for fully numerical evolutions of orbiting black-hole binaries without excision to model the last orbit and merger of an equal-mass black-hole system. We track the trajectories of the individual apparent horizons and find that the binary completed approximately one and a third orbits before forming a common horizon. Upon calculating the complete gravitational radiation waveform, horizon mass, and spin, we find that the binary radiated 3.2% of its mass and 24% of its angular momentum. The early part of the waveform, after a relatively short initial burst of spurious radiation, is oscillatory with increasing amplitude and frequency, as expected from orbital motion. The waveform then transitions to a typical ‘plunge’ waveform; i.e. a rapid rise in amplitude followed by quasinormal ringing. The plunge part of the waveform is remarkably similar to the waveform from the previously studied ‘ISCO’ configuration. We anticipate that the plunge waveform, when starting from quasicircular orbits, has a generic shape that is essentially independent of the initial separation of the binary.

PACS numbers: 04.25.Dm, 04.25.Nx, 04.30.Db, 04.70.Bw

## I. INTRODUCTION

The study of the late orbital stage of black-hole binaries is of particular interest because they are thought to be the most likely sources detected by gravitational wave observatories such as LISA [1] and LIGO [2] (which is now reaching its design sensitivity). Besides, the two body problem in General Relativity is, in itself, a genuinely interesting theoretical problem. Studies of families of binary-black-hole initial data in quasicircular orbits set the periods of the innermost stable circular orbit (ISCO) to  $37M$  for the Bowen-York family of initial data [3, 4],  $57M$  for the Thin-Sandwich family [5, 6], and  $49M$  from third-order post-Newtonian approximation (3PN) [7]. Evolution of binary black holes from these locations lead to plunge motion [8, 9, 10]; performing a fraction of an orbit before a common horizon encompasses the two black holes (i.e. forming a single, distorted black holes).

There have been several remarkable advancements in Numerical Relativity in the past few years, and, particularly since the work of [11, 12, 13], it now seems possible to evolve orbiting black-hole binaries out from arbitrary distances to the merger and ringdown. The first major breakthrough in numerical evolutions of these systems was reported by Brüggmann et. al. [14]. Using a careful choice of corotating shift and singularity excision, they were able to evolve a black-hole binary, starting from initial data for a quasicircular binary, for more than a complete orbit. Their work was recently verified by Diener et. al. [15]. However, in both cases it was not possible to extract the waveform from the merger. The first fully numerical evaluation of the waveform from an orbiting black-hole binary was reported by Pretorius [13]. Pretorius evolved a system in which two scalar fields collapsed to form individual black holes, which then formed

a merging elliptical binary. The evolution used a direct discretization of a second order in time system with singularity excision. Recently, a new technique [11, 12] has been developed for evolving black-hole binaries that uses the more conventional BSSN [16, 17, 18] system of equations (which are first-order in time). This new technique is based on the puncture approach, but allows the singular punctures to move across the grid. Singularity excision is not required and the new system has the advantages that it is very easy to implement and appears to be very accurate. This is explicitly demonstrated in Ref. [19] where this technique was applied to study the merger kicks of unequal-mass black hole binaries verifying those previously computed in Ref. [20].

We use this new ‘moving puncture’ approach to evolve the same initial configuration as in [14] and confirm that the system does indeed undergo more than a full orbit before a common horizon forms. We were also able to accurately extract the waveform and final horizon parameters. We find very good agreement in the radiated energy, angular momentum, and merger time between those calculated from the horizon properties and from the waveform.

## II. FORMULATION

Our simulations of orbiting black-hole binaries are based on a modification to the standard puncture approach. In the puncture approach [21] the metric on the initial slice is given by [22]  $\gamma_{ab} = (\psi_{BL} + u)^4 \delta_{ab}$ , where  $\psi_{BL} = 1 + \sum_{i=1}^n m_i / (2r_i)$  is the Brill-Lindquist conformal factor,  $m_i$  is the mass parameter of puncture  $i$ ,  $r_i$  is the coordinate distance to puncture  $i$ , and  $u$  is finite on the punctures.

In the standard puncture approach the locations of the

punctures are fixed (one imposes that the shift vanishes at the puncture location), and the singular behavior (i.e.  $\psi_{BL}$ ) in the metric is handled analytically. A consequence of fixing the punctures is that the coordinates become highly distorted, and this, in turn, causes numerical runs of orbiting black holes (without excision or corotation) to crash relatively early. In a recent paper we introduced a new technique for evolutions with moving punctures [11] (see [12] for an alternative implementation). This new technique, which is based on the BSSN formulation of General Relativity [16, 17, 18], does not require either excision or a corotating shift. Our technique replaces the BSSN conformal exponent  $\phi$ , which is infinite on the punctures, with the  $C^4$  field  $\chi = \exp(-4\phi)$ . This new variable, along with the other BSSN variables, will remain finite provided that one uses a suitable choice for the gauge.

We obtained accurate, convergent waveforms by evolving this system in conjunction with a modified 1+lug lapse, a modified Gamma-driver shift condition [11, 23], and an initial lapse set to  $\alpha = \psi_{BL}^{-2}$ . The lapse and shift are evolved with

$$\partial_0 \alpha = -2\alpha K, \quad (1)$$

$$\partial_t \beta^a = B^a, \quad \partial_t B^a = 3/4 \partial_t \tilde{\Gamma}^a - \eta B^a. \quad (2)$$

We use the *LazEv* framework [24] to numerically evolve this new system. Unlike in the fixed puncture approach, we do not reduce the order of finite differencing near the punctures. We use the standard centered fourth-order stencils for all derivatives except for the advection terms (i.e. terms of the form  $\beta^i \partial_i$ ) where we use upwinded fourth-order stencils. These stencils were modified near the boundary. At the second point from the boundary we use fourth-order centered stencils for all derivatives, and at the first point from the boundary, we use second-order centered stencils. We use the standard fourth-order Runge-Kutta algorithm for the time evolution and radiative boundary conditions for all evolved variables.

### III. INITIAL CONFIGURATION

Following [14] we choose black hole initial data from a quasicircular sequence [25] with parameters

$$\begin{aligned} m/M &= 0.47656, & P/M &= 0.13808, & Y/M &= \pm 3.0, \\ L/M &= 9.32, & J/M^2 &= 0.82843, & M\Omega &= 0.054988, \end{aligned}$$

where  $m$  is the mass of each single black hole,  $M = 1$  provides the scale,  $P$  is the magnitude of the linear momenta (equal but opposite and perpendicular to the line connecting the holes),  $(0, Y, 0)$  is the coordinate location of the punctures,  $L$  is the proper distance between the apparent horizons,  $J$  is the total angular momentum, and  $\Omega$  is the orbital frequency. We use the Brandt-Brügmann approach along with the BAM\_Elliptic [22, 26] Cactus thorn to solve for these initial data. The total ADM mass for this configuration is  $M_{ADM} = 0.98461M$ .

The initial choice for the lapse is  $\alpha = \psi_{BL}^{-2}$  and the initial choice for the shift is  $\beta^i = B^i = 0$ .

We evolved these data with grid resolutions of  $M/21$ ,  $M/24$ , and  $M/27$ ; and gridsizes of  $224^2 \times 448$ ,  $256^2 \times 512$ , and  $288^2 \times 576$  respectively (we exploited the  $\pi$ -rotation symmetry about the  $z$  axis and reflection symmetry about the equatorial plane to halve the number of grid-points in the  $x$  and  $z$  directions). We used a ‘multiple transition’ Fisheye transformation, which is an extension of the ‘transition’ Fisheye transformation [23, 27], to place the boundaries at  $114M$ . The ‘multiple transition’ transformation has the form  $R = Cr$ , where  $R$  is the physical radius corresponding to the coordinate radius  $r$ ,

$$C = a_n + \sum_{i=1}^n \kappa_i / r \log \left( \frac{\cosh((r + r0_i)/s_i)}{\cosh((r - r0_i)/s_i)} \right), \quad (3)$$

$$\kappa_i = \frac{(a_{i-1} - a_i)s_i}{2 \tanh(r0_i/s_i)}, \quad (4)$$

$n$  is the number of transitions,  $a_i$  is the deresolution parameter in region  $i$ ,  $a_0$  is the central resolution,  $r0_i$  is the center of the  $i$ th transition, and  $s_i$  is the width of the  $i$ th transition. For these runs we used the parameters,  $n = 2$ ,  $a_0 = 1$ ,  $a_1 = 5$ ,  $a_2 = 30$ ,  $r0_1 = 5$ ,  $r0_2 = 7.5$ ,  $s_1 = s_2 = 0.75$ . We also evolved these data with a resolution of  $M/21$  and a gridsize of  $288^2 \times 576$ , which placed the boundary at  $176.6M$ , to quantify the dependence of the results on the location of the boundary. For this run we used the Fisheye parameters,  $n = 1$ ,  $a_0 = 1$ ,  $a_1 = 25$ ,  $r0_1 = 7.0$ ,  $s_1 = 25$ .

## IV. RESULTS

We used Jonathan Thornburg’s AHPfinderDirect thorn [28] to find apparent horizons. The (coordinate) time of first appearance of the common horizon depends on resolution, with  $T_{cah} = 111M$  for the  $M/21$  run,  $T_{cah} = 113M$  (estimated) for  $M/24$ , and  $T_{cah} = 114.3$  (estimated) for the  $M/27$  run. An extrapolation of these data to infinite resolution puts the appearance of the first common horizon at  $T_{cah} = 125M$ . The common horizon has an irreducible mass of  $M_{irr} = (0.8848 \pm 0.0002)M$  and specific spin (measured from the distortions of the horizon) of  $\tilde{a} = J_{\mathcal{H}}/M_{\mathcal{H}}^2 = 0.688 \pm 0.001$ . These parameters correspond to a horizon mass of  $M_{\mathcal{H}} = (0.952 \pm 0.002)M$  and angular momentum  $J_{\mathcal{H}} = (0.6232 \pm 0.003)M^2$ . Hence  $(3.3 \pm 0.2)\%$  of the mass and  $(24.7 \pm 0.4)\%$  of the angular momentum are radiated away.

Figure 1 shows the tracks of the punctures, the individual horizons every  $10M$  of evolution, and the first common horizon. The plot was generated using the  $M/21$  resolution run with the boundaries at  $176.6M$ . In addition the plot shows the puncture trajectory for the  $M/27$  resolution run. Note that the binary completes one and a third orbits before the common horizon forms

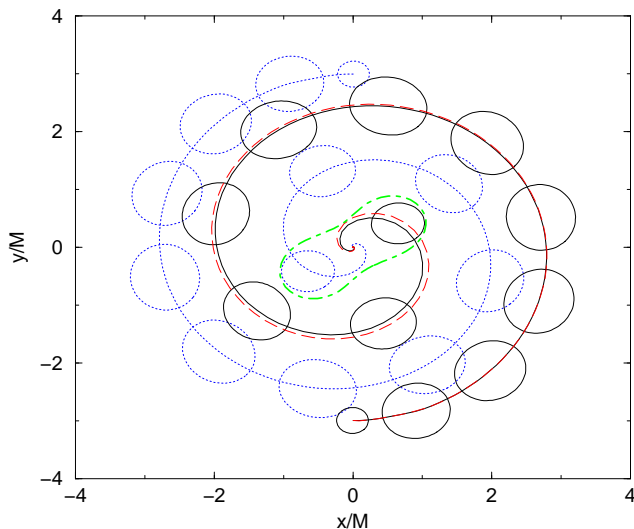


FIG. 1: The puncture trajectories and apparent horizon profiles on the  $xy$  plane for the  $M/21$  run. The solid and dotted spirals are the puncture trajectories, the solid and dotted ellipsoids are the individual apparent horizons (at every  $10M$  of evolution), the dot-dash ‘peanut shaped’ figure is the first detected common horizon, and the dashed spiral is the puncture trajectory for the  $M/27$  run. The initial growth of the individual apparent horizon is due to the non-ideal (vanishing) initial data for the shift. Note that we track the puncture positions throughout the evolution. The period of the last orbit is around  $62M$ . The last orbit begins when the punctures are located at  $2.6M$  from the origin.

(although we caution the reader that tracks are gauge dependent). The period of the last orbit is approximately  $62M$ . The puncture trajectories were calculated by integrating  $\partial_t x_{punct}^i = -\beta_{punct}^i$ , where  $\beta_{punct}^i$  is the interpolated value of the shift on the puncture (the puncture never lies on a gridpoint). The last orbit begins when the punctures are located at  $2.6M$  from the origin in the coordinate conformal space.

We use the Zorro thorn [24, 27] to calculate  $\psi_4$  and decompose it into spherical harmonics of spin weight  $-2$ . The two dominant modes are  $(\ell = 2, m = +2)$  and  $(\ell = 2, m = -2)$ , where the coefficient of the two modes are complex conjugates. Figure 2 shows the  $(\ell = 2, m = 2)$  mode of  $\psi_4$  at  $r = 20M$  for the three resolutions and a convergence plot of these data. The waveforms converge to fourth-order up to  $t = 141M$  (the convergence rate past  $t = 141M$  is obscured by the large phase error, but is better than second-order). The oscillation in  $\psi_4$  around  $t = 26M$  is due to spurious radiation in the initial data. This spurious radiation quickly leaves the system and becomes smaller than the orbital waveform at  $t \sim 50M$ . Hence the radiation from the last orbit, which begins at  $t \sim 50M$  as seen by our observer located at the radial coordinate  $r = 20M$  (see Figure 1), is essentially uncontaminated. We find that the  $(\ell = 2, m = 2)$  quasi-normal mode, for the  $M/21$  resolution run with distant

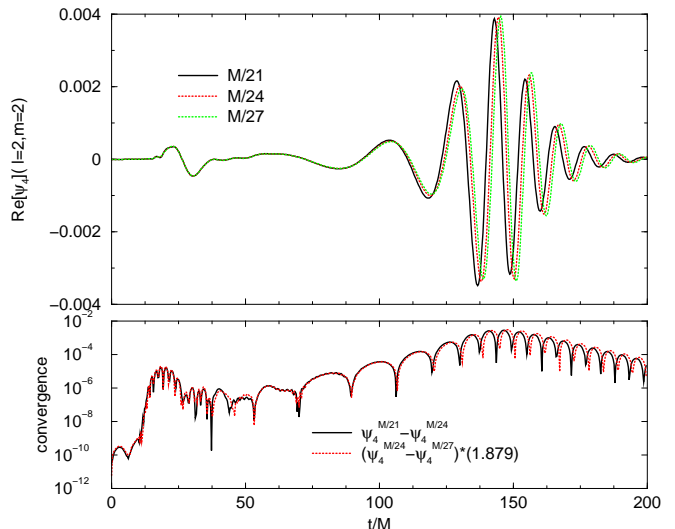


FIG. 2: The  $(\ell = 2, m = 2)$  mode of  $\psi_4$  at  $r = 20M$ . The top plot shows the waveforms for central resolutions of  $M/21$ ,  $M/24$ , and  $M/27$ . The bottom plot shows the differences  $\psi_4(M/21) - \psi_4(M/24)$  and  $\psi_4(M/24) - \psi_4(M/27)$ , with the latter rescaled by 1.879 to demonstrate fourth-order convergence. Note the spurious radiation around  $t = 26M$ .

boundaries, has a frequency of  $M_{\mathcal{H}} \omega / \alpha_{20} = 0.549 \pm 0.001$  ( $\alpha_{20} = 0.954$  is the average value of the lapse at  $r = 20M$  at late times). The reported error is from the fit to a damped sinusoidal function and does not include finite difference errors. This frequency corresponds [29] to a specific spin of  $\tilde{a} = J_{\mathcal{H}} / M_{\mathcal{H}}^2 = 0.673 \pm 0.002$ . We can also estimate when the first common horizon forms by calculating the offset between the tallest peak in the plunge waveform for these data and that of the ‘ISCO’ (as determined by the effective potential method) initial data. In a previous paper [11] we found that a common horizon forms in the ‘ISCO’ case at  $t = 19.333M$ . From these offsets we estimate that the first common horizon should form at  $111.5M$  for the  $M/21$  run,  $112.9M$  for the  $M/24$  run, and  $113.7M$  for the  $M/27$  run. These numbers are within  $0.6M$  agreement with those determined directly from the apparent horizon finder. An extrapolation of these estimates for the formation of the common horizon yields  $T_{cah} = 121.5M$ .

We calculated the radiated energy and angular momentum from  $\psi_4$  at  $r = 15M$ ,  $r = 20M$ ,  $r = 25M$ , and  $r = 30M$ . We then extrapolated these data (based on a least squares fit versus  $\rho = 1/r$ ) and found that extrapolated radiated energy and angular momentum were  $(3.18 \pm 0.2)\%$  and  $(24.3 \pm 2)\%$  respectively. Notably, these results are in excellent agreement with those calculated from the horizon mass and angular momentum. Table I summarizes the physical parameters extracted independently from the horizon and waveform.

The plunge part of the waveform shows remarkable similarities with the waveform from the ISCO. Figure 3

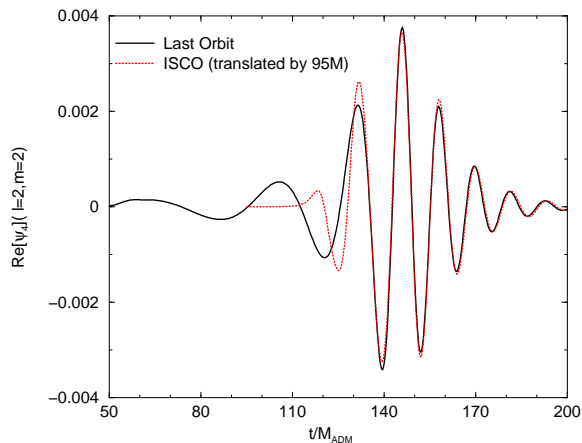


FIG. 3: The real part of the  $(\ell = 2, m = 2)$  mode of the  $\psi_4$  at  $r = 20M$  from this ‘last orbit’ configuration and from the ISCO configuration. Note the near perfect overlap once the ISCO waveform has been translated by  $\Delta t/M = 95$

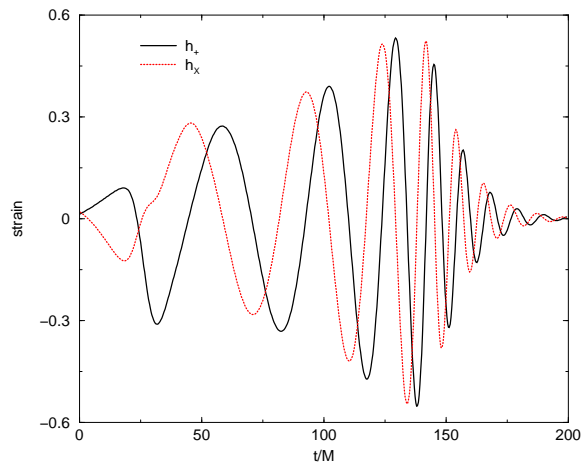


FIG. 4: The  $(\ell = 2, m = 2)$  component of the strain. Both the  $+$  and  $\times$  mode are shown. The early time strain is dominated by spurious radiation (from the initial data) up to  $t = 55M$ . Afterwards, the strain shows a gradual transition from orbital motion to a plunge waveform. This transition is less distinct than that in  $\psi_4$ .

shows the real part of the  $(\ell = 2, m = 2)$  mode for these two configurations. Note that, after a translation, there is near perfect overlap of the late-time waveform.

The gravitational strain  $h$  is related to  $\psi_4$  by  $\psi_4 = -1/2 \partial_t^2 h(t)$ . In Fig. 4 we show the  $(\ell = 2, m = 2)$  component of both polarizations of the strain. The early part of the strain ( $t < 55M$ ) is dominated by the spurious radiation of the initial data. Note that the strain amplitude and frequency shows a far more gradual transition from an orbital inspiral type waveform to a plunge type waveform than  $\psi_4$  and seems better suited to match to post-Newtonian waveforms.

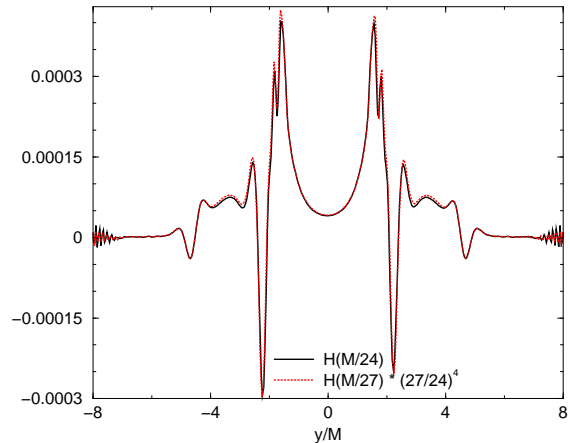


FIG. 5: The Hamiltonian constraint violation at  $t = 70M$  along the  $y$ -axis for the  $M/24$  and  $M/27$  runs (the latter rescaled by  $(27/24)^4$ ). The punctures crossed the  $y$ -axis for the second time at  $t = 64M$ . Note the near perfect fourth-order convergence. Points contaminated by boundary errors have been excluded from the plot. The high frequency violations near the numerical coordinate  $y = \pm 8$  are due to the extreme fisheye deresolution near the boundary, and converge with resolution.

TABLE I: Results of the evolution as determined from the waveform and the remnant horizon.

Method	$E_{rad}/M_{ADM}$	$J_{rad}/J_{ADM}$	$T_{cah}/M$	$a/M_{\mathcal{H}}$
Radiation	$(3.18 \pm 0.2)\%$	$(24.3 \pm 2)\%$	$\approx 121$	$0.673 \pm 0.002$
Horizon	$(3.3 \pm 0.2)\%$	$(24.7 \pm 0.4)\%$	$\approx 125$	$0.688 \pm 0.001$

To demonstrate consistency with the General Relativity field equations, we calculated the Hamiltonian constraint violation. The constraint converges to fourth-order outside of a small region surrounding the puncture (the Hamiltonian constraint violation on the nearest neighboring points to the puncture are roughly independent of resolution, but this non-converging error does not propagate outside the individual horizons). Figure 5 shows the Hamiltonian constraint violation along the  $y$ -axis at  $t = 70M$  (about  $4M$  after the punctures cross the  $y$  axis for the second time). The constraint is fourth order convergent everywhere but at points contaminated by boundary errors (these points have been removed from the plot).

## V. DISCUSSION

Using our new technique that allows punctures to move in the numerical grid, we have succeeded in accurately computing the last orbit of a black-hole binary, obtained waveforms and extracted relevant physical information such as energy and angular momentum radiated, apparent horizon geometry, and orbital parameters. These re-

sults are consistent with each other, as summarized in Table I. We also note the interesting fact that the plunge part of the waveforms (corresponding to the highest amplitude region in  $\psi_4$ ) is roughly insensitive to the initial separation of the holes when starting from a quasicircular orbit (see Fig. 3 here and Fig. 30 in Ref. [9])

When evolving the same initial configuration, Brüggmann et. al. [14] did not find a common horizon (they evolved to  $185M$ ), and concluded that the binary must have undergone at least one orbit since the orbital period of the initial configuration is around  $120M$ . Recently, Diener et. al. [15] evolved this system with various choices for the gauge (all containing a corotating shift) and concluded that a common horizon forms at about  $120M - 125M$  (after the binary completes a full orbit). They get these estimates by evolving with the extremely high resolutions of  $M/66$  and  $M/80$ , and extrapolating to the continuum limit. They compute the trajectory of the apparent horizons and find that the orbital period of the last full orbit is  $59M$ . In both [14] and [15] waveform extraction was not possible. In our work we find, like Diener et. al., that the common horizon forms between  $120M$  and  $125M$ , and that the orbital period of the last orbit is approximately  $62M$ . However, we only required a resolution as high as  $M/27$ , and could calculate accurate waveforms.

Aside from the duration of the last orbit, we estimate that the initial separation of the black holes in the final orbit is  $5.2M$  in conformal coordinates. It is interesting to compare this separation with those of several ISCO determinations. For Bowen-York initial data (as was used in this paper) the ISCO separation [3, 4] is  $2.3M$ , for Thin-Sandwich data [5, 6] it is  $3.25M$ , and an estimate of the 3PN [9] ISCO puts the separation at  $4.24M$ . Obviously, radiation reaction, which was not taken into account in those computations, leads to radial motion that plays an important role in the dynamics of the last orbit of black-hole binaries.

### Acknowledgments

We thank Erik Schnetter for providing the thorns to implement Pi-symmetry boundary conditions. We gratefully acknowledge the support of the NASA Center for Gravitational Wave Astronomy at University of Texas at Brownsville (NAG5-13396) and the NSF for financial support from grants PHY-0140326 and PHY-0354867. Computational resources were performed by the 64-node Funes cluster at UTB.

- 
- [1] K. Danzmann and A. Rudiger, *Class. Quant. Grav.* **20**, S1 (2003).
  - [2] R. Vogt, in *Sixth Marcel Grossman Meeting on General Relativity (Proceedings, Kyoto, Japan, 1991)*, edited by H. Sato and T. Nakamura (World Scientific, Singapore, 1992), pp. 244–266.
  - [3] G. B. Cook, *Phys. Rev. D* **44**, 2983 (1991).
  - [4] T. W. Baumgarte, *Phys. Rev. D* **62**, 024018 (2000), gr-qc/0004050.
  - [5] G. B. Cook and H. P. Pfeiffer, *Phys. Rev. D* **70**, 104016 (2004), gr-qc/0407078.
  - [6] M. D. Hannam, *Phys. Rev. D* **72**, 044025 (2005), gr-qc/0505120.
  - [7] L. Blanchet, *Phys. Rev. D* **65**, 124009 (2002), gr-qc/0112056.
  - [8] J. Baker, B. Brüggmann, M. Campanelli, C. O. Lousto, and R. Takahashi, *Phys. Rev. Lett.* **87**, 121103 (2001), gr-qc/0102037.
  - [9] J. Baker, M. Campanelli, C. O. Lousto, and R. Takahashi, *Phys. Rev. D* **65**, 124012 (2002), astro-ph/0202469.
  - [10] J. Baker, M. Campanelli, C. O. Lousto, and R. Takahashi, *Phys. Rev. D* **69**, 027505 (2004).
  - [11] M. Campanelli, C. O. Lousto, P. Marronetti, and Y. Zlochower (2005), gr-qc/0511048.
  - [12] J. G. Baker, J. Centrella, D.-I. Choi, M. Koppitz, and J. van Meter (2005), gr-qc/0511103.
  - [13] F. Pretorius, *Phys. Rev. Lett.* **95**, 121101 (2005), gr-qc/0507014.
  - [14] B. Brüggmann, W. Tichy, and N. Jansen, *Phys. Rev. Lett.* **92**, 211101 (2004), gr-qc/0312112.
  - [15] P. Diener et al. (2005), gr-qc/0512108.
  - [16] T. Nakamura, K. Oohara, and Y. Kojima, *Prog. Theor. Phys. Suppl.* **90**, 1 (1987).
  - [17] M. Shibata and T. Nakamura, *Phys. Rev. D* **52**, 5428 (1995).
  - [18] T. W. Baumgarte and S. L. Shapiro, *Phys. Rev. D* **59**, 024007 (1999), gr-qc/9810065.
  - [19] F. Herrmann, D. Shoemaker, and P. Laguna (2006), gr-qc/0601026.
  - [20] M. Campanelli, *Class. Quant. Grav.* **22**, S387 (2005), astro-ph/0411744.
  - [21] B. Brüggmann, *Int. J. Mod. Phys. D* **8**, 85 (1999), gr-qc/9708035.
  - [22] S. Brandt and B. Brüggmann, *Phys. Rev. Lett.* **78**, 3606 (1997), gr-qc/9703066.
  - [23] M. Alcubierre, B. Brüggmann, P. Diener, M. Koppitz, D. Pollney, E. Seidel, and R. Takahashi, *Phys. Rev. D* **67**, 084023 (2003), gr-qc/0206072.
  - [24] Y. Zlochower, J. G. Baker, M. Campanelli, and C. O. Lousto, *Phys. Rev. D* **72**, 024021 (2005), gr-qc/0505055.
  - [25] W. Tichy and B. Brüggmann, *Phys. Rev. D* **69**, 024006 (2004), gr-qc/0307027.
  - [26] cactus\_web, cactus Computational Toolkit home page: <http://www.cactuscode.org>.
  - [27] J. Baker, M. Campanelli, and C. O. Lousto, *Phys. Rev. D* **65**, 044001 (2002), gr-qc/0104063 (misprints corrected, 2005).
  - [28] J. Thornburg, *Class. Quantum Grav.* **21**, 743 (2004), gr-qc/0306056, URL <http://stacks.iop.org/0264-9381/21/743>.
  - [29] F. Echeverria, *Phys. Rev. D* **40**, 3194 (1989).

